# Perturbative QCD effects and the search for a H → WW → ℓνℓν signal at the Tevatron

**Charalampos Anastasiou,**[a] **Günther Dissertori,**[b] **Massimiliano Grazzini,**[c] **Fabian Stöckli**[b] **and Bryan Webber**[d,e]

[a] *Institute for Theoretical Physics, ETH Zurich,*
*8093 Zurich, Switzerland*

[b] *Institute for Particle Physics, ETH Zurich,*
*8093 Zurich, Switzerland*

[c] *INFN, Sezione di Firenze and Dipartimento di Fisica, Università di Firenze,*
*I-50019 Sesto Fiorentino, Florence, Italy*

[d] *Cavendish Laboratory,*
*Cambridge CB3 0HE, U.K.*

[e] *Physics Department, CERN,*
*1211 Geneva 23, Switzerland*

*E-mail:* babis@cern.ch, dissertori@phys.ethz.ch, grazzini@fi.infn.it, fabstoec@phys.ethz.ch, webber@hep.phy.cam.ac.uk

ABSTRACT: The Tevatron experiments have recently excluded a Standard Model Higgs boson in the mass range $160\,\text{GeV} < m_\text{H} < 170\,\text{GeV}$ at the 95% confidence level. This result is based on sophisticated analyses designed to maximize the ratio of accepted signal to background. In this paper we study the production of a Higgs boson of mass $m_\text{H} = 160\,\text{GeV}$ in the $gg \to \text{H} \to \text{WW} \to l\nu l\nu$ channel. We choose a set of cuts like those adopted in the experimental analysis and compare kinematical distributions of the final state leptons computed in NNLO QCD to lower-order calculations and to those obtained with the event generators PYTHIA, HERWIG and MC@NLO. We also show that the distribution of the output from an Artificial Neural Network obtained with the different tools does not show significant differences. However, the final acceptance computed with PYTHIA is smaller than those obtained at NNLO and with HERWIG and MC@NLO. We also investigate the impact of the underlying event and hadronization on our results.

## Contents

## 1 Introduction

Clarifying the role of Higgs bosons in the breaking of electroweak symmetry is of paramount importance in improving our understanding of elementary particle interactions. The discovery of the Standard Model Higgs boson, or its equivalent in theories beyond the Standard Model, is a principal objective of the high-energy collider experimental program.

Now is a very exciting time in the Higgs search since the Tevatron experiments have become sensitive to potential signals from a Higgs boson with production cross-sections of roughly the magnitude predicted by the Standard Model (SM). Both CDF [1, 2] and DØ [3] have presented studies where a cross-section about $1.5 - 1.7$ times the SM prediction for a Higgs boson with a mass about twice the W-mass can be excluded by the two experiments independently with a confidence level of 95%. Recent preliminary combinations [4, 5] of the two experiments exclude a SM Higgs boson in the mass range $160 - 170\,\mathrm{GeV}$ with a 95% confidence level. In this mass range, a signal is predominantly produced in the SM via the gluon fusion process $\mathrm{p\bar{p}} \to \mathrm{H} \to \mathrm{WW} \to ll\nu\nu$.

Higher order calculations for the background processes and especially the signal cross-section are indispensable for the study or exclusion of high mass Higgs bosons at the Tevatron. The magnitude of QCD corrections for the dominant signal process is extraordinarily large; the inclusive cross-section at next-to-next-to-leading order (NNLO) for gluon fusion is about three times larger than the leading order (LO) cross-section. This is an even larger $K$-factor than that obtained at LHC energies. The Tevatron experiments are

sensitive to a Standard Model Higgs boson signal in the mass region where gluon fusion is dominant, due to this particularly large $K$-factor and the small theoretical uncertainty which is attained with calculations at higher orders in perturbation theory.

Next-to-leading order (NLO) corrections have been computed in [6–8], where the anomalously large higher order effects in gluon fusion were first shown. The NNLO corrections for the inclusive cross-section have been computed in [9–11]. The NNLO computation has been consistently improved by resumming the soft-gluon contributions up to next-to-next-to-leading logarithmic (NNLL) accuracy [12]. The result is an additional increase of the cross section that amounts to about 13% at the Tevatron. The NNLL result is nicely confirmed by the computation of additional soft terms to N$^3$LO [13–15] (see also [16–18]). A calculation based on a somewhat different approach has been presented in ref. [19].

The calculations of threshold effects have provided an invaluable argument that by now the bulk of the higher order corrections is accounted for. Smaller theoretical effects can also be important for setting a precise exclusion limit on the Higgs boson cross-section at the Tevatron. Two-loop electroweak corrections (of about $\sim 5\%$) for gluon fusion Higgs production have been computed in [20–22] , and the full two-loop amplitude has been presented in [23, 24]. Mixed QCD and Electroweak corrections have been computed in [25]. Recent predictions for the inclusive cross-section taking into account these effects have been presented in [25, 26]; these theoretical results for the inclusive gluon fusion cross-section have been used in setting the exclusion limits of ref. [5].

Electroweak corrections of $\mathcal{O}(\alpha)$ for the decay H $\to$ WW $\to \ell\nu\ell\nu$ have been computed in [27]. These reach 6% for the partial decay width of the decay of a Higgs boson to four leptons with mass of 170 GeV. In the region just above $m_{\mathrm{H}} > 2M_{\mathrm{W}}$, which is relevant for the recent Tevatron exclusion limits, ref. [27] reported important differences with the prediction of the program HDECAY [28]. These corrections have not yet been included into estimates of the Higgs branching ratio to leptons, and they are not considered in the experimental analysis of refs. [4, 5].

The extraction of limits on the Higgs boson cross-section from the study of the H $\to$ WW $\to \ell\nu\ell\nu$ process requires a sophisticated analysis. Background processes, such as direct $WW, WZ, ZZ$ production as well as $t\bar{t}, W\gamma$ and $W+$ (multi)jet production, are dominant. Experimental cuts can suppress background and enhance the signal by vetoing hadronic radiation and by exploiting characteristic differences in lepton angular distributions as well as the large missing transverse momentum in signal events [29].

At the Tevatron, a cut-based analysis alone is not sufficient. Additional methods that exploit efficiently the kinematic features of signal and background processes in their finest detail are required. CDF [2] and DØ [3] apply cuts on missing energy and jet activity and impose lepton isolation criteria only for purposes of a first rough selection which biases the data samples towards signal events. After this first cut-based selection, background processes remain dominant and processing of real data and Monte-Carlo simulations with Artificial Neural Network (ANN) methods follows. It is easy to appreciate the importance of ANN techniques for setting exclusion limits at the Tevatron. For example, in a data sample analyzed passing first cut selection in ref. [3], the data model employed there predicts only $\sim 12$ signal versus $\sim 337$ background $e^{\pm}\mu^{\mp}$ events.

Given the sensitivity of the gluon fusion cross-section to higher order effects, it is important to establish that the sophisticated methods used in the Tevatron analysis [5] account for these effects within the estimated uncertainties. Already the first cut selection may change the relative importance of higher order corrections for signal and background cross-sections with respect to the perturbative patterns observed in the inclusive cross-sections. A complete simulation of the experimental analysis with NLO and NNLO perturbative corrections is not practically feasible. In this paper, we aim to provide precise predictions for the production cross section in conditions close to those of the actual experiments by combining knowledge of higher-order effects from fixed-order perturbation theory and parton shower event generators.

First, we provide fixed-order predictions which are sufficiently detailed to permit assessment of the sensitivity of the acceptance due to selection cuts. For such a study, fully differential cross-sections of the signal at NNLO are required. Unlike NLO computations, NNLO differential calculations are a rarity due to their substantial technical complications. The first differential distribution at NNLO was computed in 2003 [30, 31], and fully differential NNLO cross-sections appeared in 2004 [32, 33]. At an electron-positron collider NNLO differential cross-sections are known only for two [32, 34] and three jet production [35–42] cross-sections. At hadron colliders fully differential cross-sections have been computed only for Higgs production in gluon fusion [33, 43–46], and the Drell-Yan process [47–49].

In this paper we compute accepted cross-sections and kinematic distributions at NNLO using the programs FEHIP [43, 45] and HNNLO [46]. We find an excellent agreement between the predictions of the two programs. We remark that the methods used [44, 50] for constructing these fully differential NNLO programs are independent and very different in their conception. Both programs produce kinematic distributions in the form of bin histograms. All NNLO results for cross-sections and kinematic distributions calculated with both programs and presented here are in agreement within the expectations of statistical integration errors. The NNLO acceptance of the selection cuts can be directly compared with the predictions from the modeling of data as it has been performed by the CDF [2] and DØ [3] collaborations. The kinematic distributions we present here are input for their ANN analyses.

Two selection cuts require special care in estimating their acceptance for the Tevatron studies: (i) a jet veto on two or more central jets and (ii) isolation of leptons from hadronic activity. These cuts are used in DØ [3] in order to define the entirety of the data sample and at CDF [2] that part of the sample with a potential Higgs boson signal. At CDF [2], a further division of the data sample into zero- and one-jet multiplicities is made. The relative magnitude of the perturbative corrections at NLO and NNLO with respect to LO ($K$-factor) is smaller after applying selection cuts.

The same observation was made in earlier NNLO studies [45, 46] of the process pp $\rightarrow$ H $\rightarrow$ WW $\rightarrow \ell\nu\ell\nu$ at LHC center-of-mass energy of 14 TeV, with similar cuts, such as a jet-veto. In a separate paper [51], these NNLO predictions at the LHC were compared to results obtained from (i) a resummation of logarithms in the transverse momentum of the Higgs boson at NNLL accuracy [52] and (ii) the Monte-Carlo event generator MC@NLO [53]. They were found to be in good agreement with each other over the phase-space regions

singled out by the event selection cuts. On the contrary, a fixed-order calculation at next-to-leading order (NLO) accuracy provided a rather poor approximation for the required distributions and cut efficiencies.

In this paper we compare the selection cut acceptance and the shape of kinematic distributions for leptons at NNLO with the event generators MC@NLO [53], HERWIG [54], and PYTHIA8 [55] for Tevatron collisions.

The simulation of the gluon fusion process in refs. [2, 3], is performed with PYTHIA6 [56]. In these analyses, the uncertainty in the acceptance after selection cuts is estimated with other means rather than a direct NNLO calculation. In the CDF analysis [2], PYTHIA events are reweighted [57, 58] to match either the (N)NLO Higgs $p_T$ or the NNLO Higgs rapidity spectrum [43, 46]. The systematic uncertainty in the acceptance is computed from the differences between the original PYTHIA and the reweighted versions. In DØ, acceptance uncertainties are estimated by comparing the spectrum of PYTHIA with that of other generators, such as MC@NLO [53] and SHERPA [59]. We believe that neither of the two methods can substitute for a direct comparison with the acceptance at NNLO. We will discuss this point in section 4.

Multivariate techniques and distributions of ANN variables have so far been "terra incognita" for theoretical calculations at higher orders in perturbation theory. To the best of our knowledge, there has been no calculation of NLO and NNLO corrections for such observables. So far, the systematic uncertainty due to higher order effects on the shape of ANN distributions has been estimated indirectly. ANNs construct composite output variables that maximize the differences between signal and background cross-sections. An error estimate on the shape of the ANN output distribution is obtained by varying the input kinematic distributions within their uncertainty range. However, if the input variables have a proper definition at the parton level, there is no obstacle to computing the corrections directly at fixed order in perturbation theory in the same fashion as for any other simple partonic variable. This should provide a more reliable theoretical estimate of the uncertainty on the ANN distribution.

We demonstrate such a calculation of an ANN output distribution through NNLO in this paper. We train an ANN with a PYTHIA simulated data sample that satisfies the selection in ref. [1], which is a similar but somewhat simpler selection than that in refs. [2, 3]. As input we use kinematic distributions of the leptons in the final state. We have deliberately refrained from using variables such as the transverse momentum of the Higgs boson or jets, since these distributions may differ substantially in event generators, and they are not defined in their full physical range in fixed order perturbation theory. We compare the predictions of PYTHIA, MC@NLO and HERWIG for this ANN output, and find reasonable agreement if the observed discrepancies at the cut selection levels are already accounted for.

The organization of the paper is as follows: We first present in section 2 our predictions for the inclusive cross section at various orders of perturbation theory, then in section 3 we define the experimental observables to which selection cuts are applied. Section 4 is devoted to a discussion of the Higgs $p_T$ spectrum and of the jet multiplicities. In section 5 we give the results for the accepted cross section, i.e. after applying cuts on the various

observables, and discuss the impact of the higher order corrections and scale variations on the selection efficiency. Next we present detailed comparisons of kinematical distributions, calculated at different orders of perturbative QCD (section 6) and by using parton shower Monte Carlo models (section 7). In section 8 we compare for the first time fixed-order and parton shower Monte Carlo predictions for the output of an artificial neural network (ANN) similar to that used by the experimental groups. We comment on the stability and accuracy of these perturbative predictions, depending on the type of input variables to the ANN. Our conclusions are summarized in section 9.

## 2   Inclusive cross section

Recent updates on the inclusive cross section for Higgs boson production at hadron colliders have been presented in refs. [25, 26].

In ref. [25], the fixed order NNLO cross-section [9–11] is recomputed with MSTW2008 parton densities [60]. Two-loop electroweak corrections from [23, 24] and exact finite top and bottom mass effects [8, 61] are included. Mixed QCD electroweak effects are taken into account by computing the relative magnitude of the correction with respect to the leading two-loop electroweak contribution by means of an effective theory. The central value of the cross-section is determined at a factorization and renormalization scale $\mu = m_{\mathrm{H}}/2$. The scale variation error for Higgs mass values $160 - 170\,\mathrm{GeV}$ in this fixed order calculation is $+7\%, -11\%$. The corresponding parton density error is $\sim \pm 10\%$.

In ref. [26], the NNLL calculation [12] with the appropriate matching to the fixed order NNLO result [9–11] is repeated using the MSTW2008 parton densities [60]. Two-loop electroweak corrections from [23, 24] and exact finite top and bottom mass effects [8] are included. Mixed QCD electroweak effects are taken into account by multiplying the inclusive two-loop electroweak contribution [23, 24] with the QCD $K$-factor. The central value of the cross-section is determined at a factorization and renormalization scale $\mu = m_{\mathrm{H}}$. The scale variation error for Higgs mass values $160 - 170\,\mathrm{GeV}$ in this resummed calculation is $+9\%, -8\%$. The corresponding parton density error is $\sim \pm 8\%$.

The central values of the cross-sections in Refs [25, 26] agree within a percent, and they have been used in setting the exclusion limits in [5]. CDF assigns a global theoretical uncertainty on the inclusive cross-section of $\pm 12\%$ [2], adding in quadrature a $\pm 11\%$ scale variation error and a $\pm 5\%$ parton density error. In our opinion, the combination of the two errors in quadrature requires further justification. DØ assigns a somewhat smaller theoretical uncertainty of $\pm 10\%$ to the inclusive Higgs boson cross-sections. Even justifying a combination in quadrature of the uncertainties from parton densities and scale variations, the uncertainties on the total rate appear underestimated, compared to those of refs. [25, 26].

The main goal of the present paper is to assess the theoretical uncertainties on the shapes of kinematic distributions and the acceptance after selection cuts. We have used MRST2001 PDFs at LO and MRST2004 PDFs at NLO and NNLO. All the fixed-order results in this paper have been obtained independently with the FEHiP [33, 43, 45, 51] and HNNLO [44, 46] programs, by first calculating $K$-factors in the limit of a very heavy top-quark and then by multiplying these $K$-factors with the exact leading order gluon fusion

| $\sigma_{\mathrm{inc}}$ [fb] | LO | NLO | NNLO | $K^{\mathrm{NLO}}$ | $K^{\mathrm{NNLO}}$ |
|---|---|---|---|---|---|
| $\mu = m_{\mathrm{H}}/2$ | $1.998 \pm 0.003$ | $4.288 \pm 0.004$ | $5.252 \pm 0.016$ | $2.149 \pm 0.008$ | $2.629 \pm 0.009$ |
| $\mu = m_{\mathrm{H}}$ | $1.398 \pm 0.001$ | $3.366 \pm 0.003$ | $4.630 \pm 0.010$ | $2.412 \pm 0.002$ | $3.312 \pm 0.008$ |
| $\mu = 2\,m_{\mathrm{H}}$ | $1.004 \pm 0.001$ | $2.661 \pm 0.002$ | $4.012 \pm 0.007$ | $2.651 \pm 0.008$ | $3.996 \pm 0.008$ |

**Table 1**. Inclusive cross sections for $m_{\mathrm{H}} = 160\,\mathrm{GeV}$, at various orders in perturbation theory and for different scale choices. The $K$-factors are defined in the text; LO=Leading order.

cross section for Higgs production via a top-quark (ignoring bottom contributions). The total width is computed using the program HDECAY [28]. $\mathcal{O}(\alpha)$ electroweak corrections for the Higgs partial decay to leptons [27] have also been ignored. This is justified for studies of shapes and acceptances.

The cross-section for $\mathrm{p\bar{p}} \to \mathrm{H} \to \mathrm{WW} \to \ell\nu\ell\nu$, with no cuts applied and using the setup described in the last paragraph, is presented in table 1 for illustration. We have chosen to study the signal cross-section for a Higgs mass value $m_{\mathrm{H}} = 160\,\mathrm{GeV}$, and we vary the renormalization ($\mu_{\mathrm{R}}$) and factorization ($\mu_{\mathrm{F}}$) scales simultaneously in the interval $\mu = \mu_{\mathrm{F}} = \mu_{\mathrm{R}} \in [m_{\mathrm{H}}/2, 2\,m_{\mathrm{H}}]$. In the same table, we also present the $K$-factors for the inclusive cross section,

$$K^{(\mathrm{N})\mathrm{NLO}}(\mu) = \frac{\sigma^{(\mathrm{N})\mathrm{NLO}}(\mu)}{\sigma^{\mathrm{LO}}(\mu)}. \tag{2.1}$$

The perturbative corrections are very large, and there is still a substantial $23-50\%$ increase, depending on the scale choice, of the cross-section at NLO upon including the NNLO corrections. The smallest $K$-factors occur for smaller values of the renormalization and factorization scale.

## 3 Observables and selection cuts

The very sophisticated and complex experimental analyses of the two Tevatron collaborations cannot be reproduced fully at a perturbative level. In addition, there are important differences between the CDF and DØ analyses, both at the event selection level and in the usage of ANNs, and they evolve with time and the acquisition of more data. Nevertheless, we believe the analysis presented here captures the essential features that allow us to study the likely sensitivity of the results to higher order effects.

Our particle and event selection follows along the lines of the CDF analysis of ref. [1] and proceeds through the following steps:

1. Lepton selection: in the CDF experiment, the experimental acceptances for electrons and muons are different. In this publication, we only consider the final state with two muons, simulating only the muon acceptance. The differences in the CDF cuts for muons and electrons are rather geometric, and should not alter the convergence pattern of the perturbative corrections. In our analysis, one of the final-state leptons (the 'trigger lepton') must have a transverse momentum $p_{\mathrm{T}} > 20\,\mathrm{GeV}$ and pseudo-

rapidity $|\eta| < 0.8$. In order to pass a further lepton selection, a second lepton must be found with $p_T > 10\,\mathrm{GeV}$ and $|\eta| < 1.1$.

(a) Two opposite-sign leptons have to be found, fulfilling the requirements discussed above.

(b) Both leptons have to be isolated, i.e. the additional transverse energy in a cone with radius $R = 0.4$ around the lepton has to be smaller than $10\,\%$ of the lepton transverse momentum.

(c) In order to reduce the background from b resonances, the invariant mass of the lepton pair has to be $m_{\ell\ell} > 16\,\mathrm{GeV}$.

2. We define the missing transverse energy (MET) as the vectorial sum of the transverse momenta of the two neutrinos. We define the variable MET$^*$ as

$$\mathrm{MET}^* = \begin{cases} \mathrm{MET} & , \ \phi \geq \pi/2 \\ \mathrm{MET} \times \sin\phi \ , & \phi < \pi/2 \end{cases}, \tag{3.1}$$

where $\phi$ is the angle in the transverse plane between MET and the nearest charged lepton or jet. We require MET$^* > 25\,\mathrm{GeV}$, which suppresses the background from Drell-Yan lepton pairs and removes contributions from mismeasured leptons or jets.

3. In order to suppress the $t\bar{t}$ background, we apply a veto on the number of jets in the event. Jets are found using the $k_T$-algorithm [63, 64] with parameter $R = 0.4$. A jet must have $p_T > 15\,\mathrm{GeV}$ and $|\eta| < 3.0$. Events are only accepted if there is no more than one such jet.

The jet veto that we apply here is different from that used in our corresponding LHC studies [45, 46, 51], where all events with any number of central jets with a $p_T$ higher than a certain minimum value are vetoed. The cuts in the present study allow for events with a single high-$p_T$ jet. This type of jet veto is used in the DØ analysis [3] in order to define the data sample with a potential Higgs signal. A stricter jet veto is applied in the CDF analysis [2], where three data samples are defined according to whether events have zero, one, or more central jets.

## 4 Higgs $p_T$ spectrum and jet multiplicities

One of the most important distributions for a Higgs boson produced at hadron colliders is its transverse momentum spectrum. A good description of the $p_T$ spectrum implies a good understanding of the QCD radiation recoiling against the Higgs.

It is well known that the Higgs $p_T$ spectrum is not physical when computed at fixed order, since it diverges to $+\infty$ or $-\infty$ at any fixed order in $\alpha_s$. When $p_T \ll m_H$ large logarithmic contributions of the form $\alpha_s^n \ln^m m_H/p_T$ appear that must be resummed to all orders. In ref. [52] the resummation of these logarithmically enhanced terms has been performed analytically up to NNLL accuracy, and the result has then been matched to the fixed order calculation up to $\mathcal{O}(\alpha_s^4)$. The integral of the ensuing spectrum coincides with
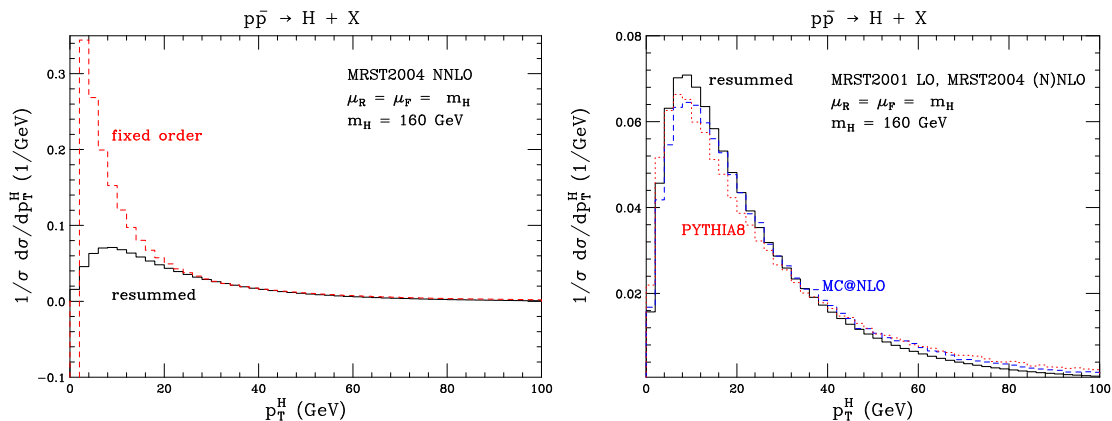
**Figure 1**. On the left figure, we show the normalized transverse momentum distributions for $m_H = 160\,\text{GeV}$ and $\mu = \mu_R = \mu_F = m_H$ using NNLO fixed-order perturbation theory and the resummed calculation of ref. [52]. On the right figure, the same distribution is shown for MC@NLO, PYTHIA8, and the calculation of ref. [52].

the total NNLO cross section. In figure 1 (left) we compare the normalized $p_T$ spectrum of the Higgs computed at fixed order, to the one obtained with the numerical program of ref. [52]. We see that the fixed order calculation diverges to $-\infty$ as $p_T \to 0$. The resummed calculation is instead well behaved as $p_T \to 0$. We also note that the two calculations are in good agreement for $p_T$ larger than about 30 GeV.

Standard Monte Carlo event generators effectively perform the transverse-momentum resummation, and thus obtain a well behaved $p_T$ spectrum. A comparison of the $p_T$ spectra from PYTHIA and MC@NLO to the resummed calculation is presented in figure 1 (right). We notice that the PYTHIA spectrum is softer than those of MC@NLO and the NNLL calculation. This difference is more marked at LHC energies [62].

We now comment on the procedure used by CDF and DØ to estimate the systematic uncertainties on the signal acceptance. The simulation of the gluon fusion process in Refs [2, 3], is performed with PYTHIA [56]. In these analyses, the uncertainty in the acceptance after selection cuts is estimated with different methods. In the CDF analysis [2], PYTHIA events are reweighted [57, 58] to match either the (N)NLO Higgs $p_T$ or the NNLO Higgs rapidity spectrum [43, 46]. The systematic uncertainty in the acceptance is computed from the differences between the original PYTHIA and the reweighted versions. In DØ, acceptance uncertainties are estimated by comparing the spectrum of PYTHIA with that of other generators, such as MC@NLO [53] and SHERPA [59]. We believe that neither of the two methods can substitute for a direct comparison with the acceptance at NNLO.

The reweighting technique used by CDF is based on the NNLO $p_T$ spectrum of the Higgs boson. As shown in figure 1, the fixed-order Higgs $p_T$ spectrum is divergent as $p_T \to 0$. A reweighting procedure based on the NNLO Higgs $p_T$ spectrum makes sense only if the signal rate is integrated over a reasonably large $p_T$ region (as is done, for example, in ref. [58]). In this respect, it would be better to reweight using a resummed calculation [52], or to use different kinematic variables.

| $\sigma$ [ fb] | LO (pdfs, $\alpha_s$) | NLO (pdfs, $\alpha_s$) | NNLO (pdfs, $\alpha_s$) |
|---|---|---|---|
| 0-jets | $3.452^{+7\%}_{-10\%}$ | $2.883^{+4\%}_{-9\%}$ | $2.707^{+5\%}_{-9\%}$ |
| 1-jet | $1.752^{+30\%}_{-26\%}$ | $1.280^{+24\%}_{-23\%}$ | $1.165^{+24\%}_{-22\%}$ |
| $\geq$ 2-jets | $0.336^{+91\%}_{-44\%}$ | $0.221^{+81\%}_{-42\%}$ | $0.196^{+78\%}_{-41\%}$ |

**Table 2**. Inclusive cross sections in the different jet bins.

Note also that a reweighting based on the Higgs $p_{\rm T}$ and rapidity is insensitive to the jet multiplicity of the event, which is used in order to divide the data sample. Another important aspect is that the relative weight of the one- and two-jet sample is enhanced by the CDF cuts, with respect to the zero-jet sample. If a jet is required in all events, the $\mathcal{O}(\alpha_s^4)$ calculation includes matrix elements through NLO only. If two jets are required, only LO matrix-elements are taken into account. An NLO prediction for 1-jet samples and a LO prediction for 2-jet samples[1] can be obtained with FEHIP and HNNLO using the corresponding NLO and LO $\alpha_s$ and parton densities. More importantly, we find it inconsistent to use the theoretical uncertainty from the inclusive NNLO gluon fusion cross-section as the uncertainty of the samples with defined jet multiplicities other than zero.

To demonstrate this point further, we follow an analogous procedure as in [2] and divide the signal cross-section into three bins according to the number of central jets. Jets are defined using the $k_{\rm T}$-algorithm, with minimum $p_{\rm T} = 15\,{\rm GeV}$ and maximum rapidity $|\eta| < 2$. We compute the inclusive cross-sections for $m_{\rm H} = 160\,{\rm GeV}$ and vary the renormalization and factorization scale simultaneously in the interval $[m_{\rm H}/2, 2m_{\rm H}]$. In table 2 we compute the three bin cross-sections, using either NNLO or NLO or LO parton densities and $\alpha_s$ evolution from the recent MSTW2008 fit [60].

The total cross-section with NNLO pdfs varies around the default scale value $\mu = m_{\rm H}$ by $\pm 14\%$. From table 2 we see that about 66.5% of the events contain zero jets, 28.6% one jet only, and 4.9% contain more than one jets. Notice, however, that the scale variation in the three jet bins is significantly different and deteriorates with increasing jet multiplicity. This is a consequence of the fact that in the 1-jet and 2-jet bins the fixed order calculation is only accurate through NLO and LO, respectively. The resulting scale dependence of the inclusive cross section is made up as follows:

$$\frac{\Delta N_{\rm inc}(\text{scale})}{N_{\rm inc}} = 66.5\% \cdot \binom{+5\%}{-9\%} + 28.6\% \cdot \binom{+24\%}{-22\%} + 4.9\% \cdot \binom{+78\%}{-41\%} = \binom{+14.0\%}{-14.3\%} \qquad (4.1)$$

The application of different selection cuts in the three jet bins leads to a theoretical error estimate of the number of signal events which is different from the theoretical error of the inclusive NNLO cross-section. Specifically, from tables 1-3 of ref. [2] we observe that, after preselection, 60% of gluon fusion events belong to the 0-jets bin, 29% to the 1-jet bin, and 11% to the 2-jet bin.

We now examine how this modification of the jet multiplicities with the experimental cuts affects the scale variation for the total number of events. With the exception of the

---

[1] An NLO calculation for $H + 2$ jets via gluon fusion can be found in [65].

| $\sigma_{\text{acc}}$ [fb] | LO | NLO | NNLO | $K^{\text{NLO}}$ | $K^{\text{NNLO}}$ |
|---|---|---|---|---|---|
| $\mu = m_{\text{H}}/2$ | $0.750 \pm 0.001$ | $1.410 \pm 0.003$ | $1.459 \pm 0.003$ | $1.880 \pm 0.005$ | $1.915 \pm 0.025$ |
| $\mu = m_{\text{H}}$ | $0.525 \pm 0.001$ | $1.129 \pm 0.003$ | $1.383 \pm 0.004$ | $2.150 \pm 0.007$ | $2.594 \pm 0.052$ |
| $\mu = 2\,m_{\text{H}}$ | $0.379 \pm 0.001$ | $0.903 \pm 0.002$ | $1.242 \pm 0.001$ | $2.383 \pm 0.008$ | $3.261 \pm 0.048$ |

**Table 3**. Accepted cross sections and $K$-factors after the application of all the selection cuts for $m_{\text{H}} = 160\,\text{GeV}$.

jet-veto, all other cuts used in the CDF preselection [2] do not affect the scale variation of the total cross-section significantly. We can then estimate the scale variation of the total number of signal events using the scale-variations for each jet-multiplicity in table 2 and the expected composition of jet-multiplicities for the signal [2]. Using NNLO pdf's and NNLO $\alpha_s$ evolution for all jet bins, we find that:

$$\frac{\Delta N_{\text{signal}}(\text{scale})}{N_{\text{signal}}} = 60\% \cdot \binom{+5\%}{-9\%} + 29\% \cdot \binom{+24\%}{-22\%} + 11\% \cdot \binom{+78\%}{-41\%} = \binom{+18.5\%}{-16.3\%} \qquad (4.2)$$

The resulting scale variation is therefore larger than the corresponding scale variation of $\pm 14\%$ for the inclusive cross-section.

Notice that in eq. (4.2) we used a scale variation for the one-jet and two-jet bins corresponding to NNLO pdfs and $\alpha_s$ evolution. A more consistent approach would be to estimate the number of events in the 1-jet and 2-jet bins using NLO and LO pdfs and $\alpha_s$ evolution correspondingly. In this way we obtain:

$$\frac{\Delta N_{\text{signal}}(\text{scale})}{N_{\text{signal}}} = 60\% \cdot \binom{+5\%}{-9\%} + 29\% \cdot \binom{+24\%}{-23\%} + 11\% \cdot \binom{+91\%}{-44\%} = \binom{+20.0\%}{-16.9\%} \qquad (4.3)$$

The relative population of the jet bins is very important for the determination of the theoretical error on the total number of events. The contribution of the different jet multiplicities to the total error can be altered also after the preselection cuts, since, in general, the independent multivariate methods for discriminating signal from background events in various jet bins should have different discriminating efficiency. In conclusion, the theoretical error for the number of events at various jet multiplicities should not be estimated collectively from the scale variation of the total cross-section.

## 5 Signal cross section and preselection efficiency at fixed order

We present in table 3 the LO, NLO, and NNLO cross sections, as obtained with FEHIP and HNNLO after applying the selection cuts in section 3, for a default Higgs boson mass value $m_{\text{H}} = 160\,\text{GeV}$.

Comparison of the results of table 3 with those of table 1 shows that the impact of QCD radiative corrections is significantly reduced when selection cuts are applied. Indeed, for $\mu_F = \mu_R = m_H$ the NLO and NNLO $K$-factors are reduced by 11% and 22%, respectively. As a consequence, the acceptance is also reduced, since it is defined as the ratio of the cross-section after cuts to the inclusive cross section. At LO about 38% of the events
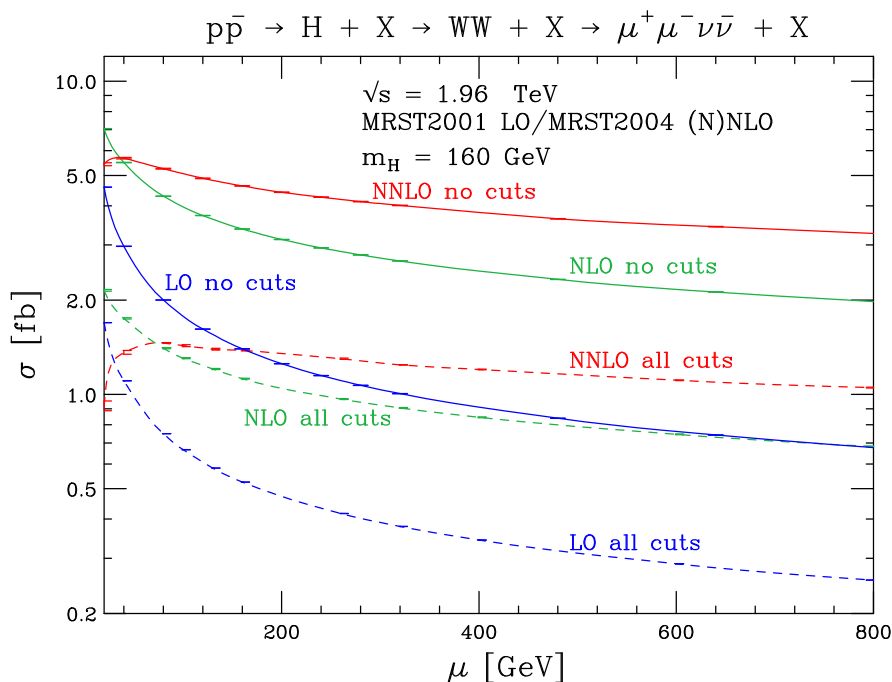
**Figure 2**. Cross sections for $m_H = 160 \, \text{GeV}$ as a function of the scales $\mu = \mu_R = \mu_F$ for different orders in fixed-order perturbation theory. The solid lines represent inclusive cross sections, the dashed lines cross sections after the application of the selection cuts.

are accepted. At NLO, the efficiency drops to $33\% - 34\%$ and at NNLO to $28\% - 31\%$, depending on the scale choice.

An important observation is that the scale dependence of the efficiency becomes stronger when we increase the perturbative order. The lepton isolation and jet-veto cuts do not change the LO cross section, since the isolation requirement gives a non-vanishing contribution only at NLO and the veto on the number of central jets is effective only beyond NLO. We will comment further on the jet-veto later when comparing to the Monte-Carlo event generators, PYTHIA, HERWIG and MC@NLO.

The increased scale variation of the acceptance at NNLO is a reflection of the reduction of the scale variation for the cross section after cuts are applied. In figure 2, we present the cross section as a function of the renormalization and factorization scale $\mu = \mu_R = \mu_F$, before and after cuts, at LO, NLO, and NNLO. Before cuts, the NNLO cross section varies by $27\%$ over the interval $[m_H/2, 2m_H]$. This drops to a $16\%$ scale variation after cuts, and consequently the ratio varies by $\sim 11\%$. We note that the scale variation in a different but also commonly used range $[m_H/4, m_H]$ is $20\%$ for the inclusive cross-section and $6\%$ for the accepted cross-section after cuts. In this second scale variation range, the accepted cross-section is not monotonic and develops a maximum.

## 6 Kinematic distributions at fixed order perturbation theory

We now turn to a more detailed study of the kinematical properties of the accepted events. The applied cuts provide a rough discrimination of the Higgs signal over the background. The experimental analysis proceeds further by exploiting the differences in the kinematical distributions between signal and background and is typically based on Artificial Neural Network (ANN) techniques. It is thus important to check that these distributions are stable against radiative corrections.

In figure 3 we present a set of distributions that are commonly used in the experimental analysis, computed at LO, NLO and NNLO. The uncertainty bands are obtained by varying $\mu_F = \mu_R$ between $m_H/2$ and $2m_H$. Figures 3(a) and (b) show the transverse momentum spectrum of the leading and trailing lepton, $p_{\mathrm{T}}^{\mathrm{hard}}$ and $p_{\mathrm{T}}^{\mathrm{soft}}$. Figure 3(c) shows the invariant mass distribution of the lepton pair, $m_{ll}$, figure 3(d) shows the MET distribution and, finally, figure 3(e) shows the azimuthal separation of the two charged leptons in the transverse plane, $\phi_{\ell\ell}$. Overall, these plots show that the distributions are quite stable when going from NLO to NNLO. The NNLO band generally lies on top of the NLO band and nicely overlaps with the latter. The scale uncertainty of the distributions is consistent with that quoted in table 3 and is about $\pm(6-8)\%$ in the peak region of the distributions.

We also observe that the perturbative corrections from NLO to NNLO are smaller when the scale $\mu = m_{\mathrm{H}}/2$ is used.

## 7 Comparison with parton shower event generators

In the next step we compare the accepted cross-section and kinematic distributions after selection cuts, obtained in fixed order perturbation theory, with the predictions of the parton shower event generators HERWIG, PYTHIA and MC@NLO. We consider this as a very important validation for the current studies at the Tevatron, which rely on event generator predictions.

In table 4 we present the predictions of the fixed order calculations through NNLO, as well as the predictions of PYTHIA, HERWIG and MC@NLO. At this stage we do not include a simulation of hadronization and the underlying event, in order to make a more direct comparison with the fixed order predictions, which cannot take into account such effects. The total inclusive cross-section of PYTHIA and HERWIG corresponds to a pure LO computation, and that of MC@NLO is correct at NLO accuracy. Since we are interested in a comparison of the efficiencies and not of absolute cross-sections, we multiply the results of the event generators with appropriate scaling factors, such that they match the result of the total inclusive cross-section given by our fixed order computation. Because of the different parton distribution functions and approximation for the top loop used in the various calculations, these scaling factors to match the leading fixed order calculations [43, 46] are different from unity at the level of 5%.

After applying the selection cuts, we find a relatively good agreement among the NNLO, MC@NLO and HERWIG results for the accepted cross-sections, with the MC@NLO and HERWIG predictions rescaled to reproduce the fixed order NNLO inclusive cross sec-
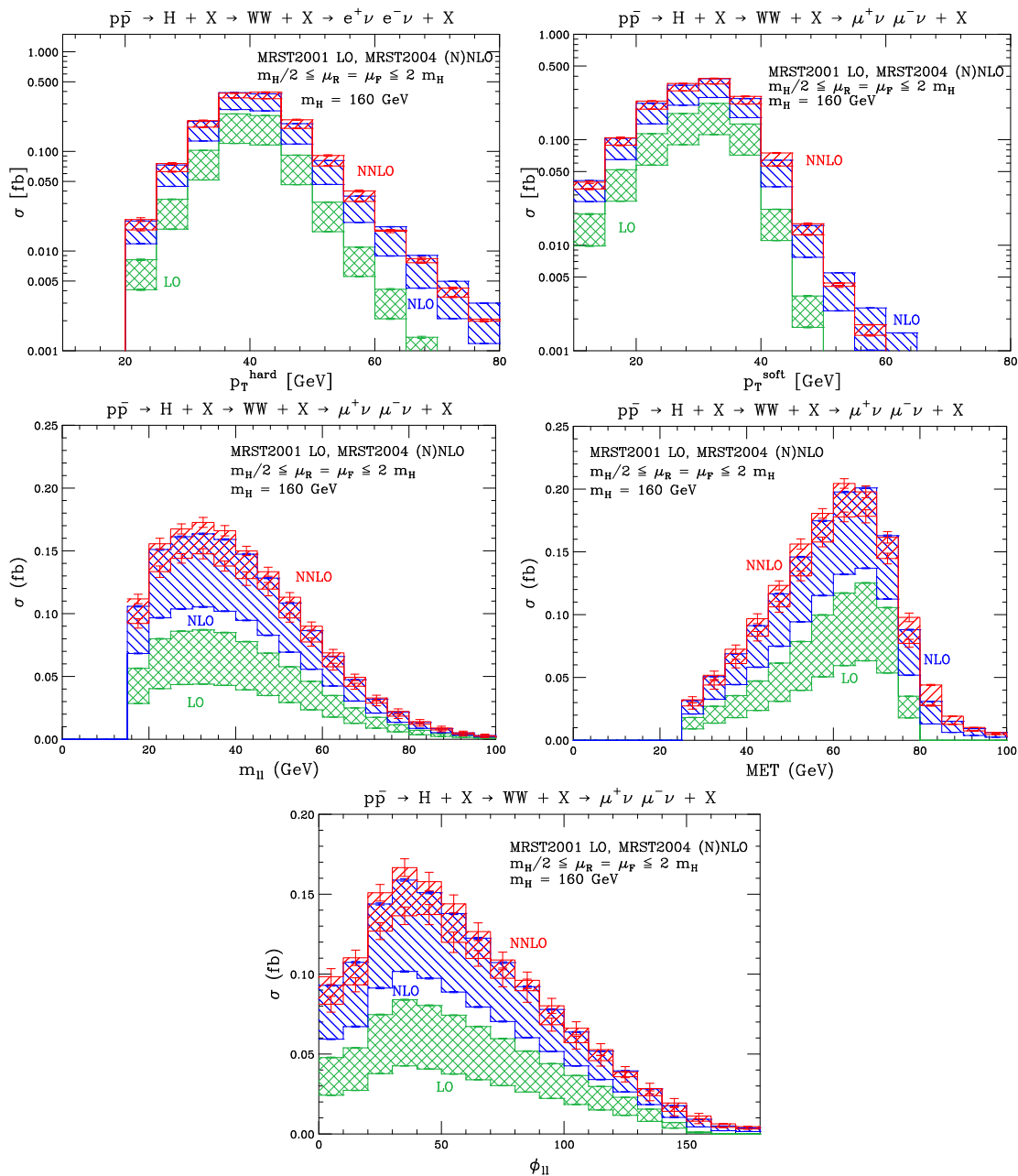
**Figure 3**. Kinematic distributions obtained at LO, NLO and NNLO in perturbative QCD. Shown are the transverse momentum of the leading ($p_T^{\text{hard}}$) and trailing lepton ($p_T^{\text{soft}}$), the invariant mass of the two leptons ($m_{ll}$), the transverse missing energy (MET) and the azimuthal separation of the two charged leptons in the transverse plane ($\phi_{\ell\ell}$).

tion before cuts, as explained above. The MC@NLO result is smaller than the NNLO prediction by $4 - 14\%$, depending on the scale choice. HERWIG results differs from the NNLO prediction by $-3\%$ to $+8\%$. On the contrary, the accepted cross section and consequently the selection efficiency obtained with PYTHIA appears to be somewhat smaller.

| $\sigma_{\text{acc}}$ [fb] | $\mu = m_{\text{H}}/2$ | $\mu = m_{\text{H}}$ | $\mu = 2\, m_{\text{H}}$ |
|---|---|---|---|
| LO | 0.750 ± 0.001 | 0.525 ± 0.001 | 0.379 ± 0.001 |
| $R^{\text{LO}}$(HERWIG) | 0.571 ± 0.001 | 0.399 ± 0.001 | 0.287 ± 0.001 |
| $R^{\text{LO}}$(PYTHIA) | 0.483 ± 0.001 | 0.338 ± 0.001 | 0.245 ± 0.001 |
| NLO | 1.410 ± 0.003 | 1.129 ± 0.003 | 0.903 ± 0.002 |
| MC@NLO | 1.143 ± 0.002 | 0.906 ± 0.003 | 0.718 ± 0.002 |
| $R^{\text{NLO}}$(HERWIG) | 1.225 ± 0.001 | 0.962 ± 0.001 | 0.760 ± 0.001 |
| $R^{\text{NLO}}$(PYTHIA) | 1.037 ± 0.002 | 0.814 ± 0.002 | 0.645 ± 0.001 |
| NNLO | 1.459 ± 0.003 | 1.383 ± 0.004 | 1.242 ± 0.001 |
| $R^{\text{NNLO}}$(MC@NLO) | 1.399 ± 0.003 | 1.246 ± 0.003 | 1.082 ± 0.003 |
| $R^{\text{NNLO}}$(HERWIG) | 1.501 ± 0.001 | 1.323 ± 0.001 | 1.146 ± 0.001 |
| $R^{\text{NNLO}}$(PYTHIA) | 1.271 ± 0.002 | 1.120 ± 0.002 | 0.971 ± 0.002 |

**Table 4**. Comparison of the accepted cross-section obtained in fixed order perturbation theory and from various event generators. The predictions from event generators are rescaled such that the predictions for the inclusive cross-section are in agreement with the corresponding fixed order result.

| $\sigma_{\text{acc}}/\sigma_{\text{incl}}$ | Trigger | + Jet-Veto | + Isolation | All Cuts |
|---|---|---|---|---|
| NNLO ($\mu = m_{\text{H}}/2$) | 44.7% | 39.4% (88.1%) | 36.8% (93.4%) | 27.8% (75.5%) |
| NNLO ($\mu = 2\, m_{\text{H}}$) | 44.9% | 41.8% (93.1%) | 40.7% (97.4%) | 31.0% (76.2%) |
| MC@NLO ($\mu = m_{\text{H}}/2$) | 44.4% | 38.1% (85.8%) | 35.3% (92.5%) | 26.5% (75.2%) |
| MC@NLO ($\mu = 2\, m_{\text{H}}$) | 44.8% | 38.8% (86.7%) | 35.9% (92.5%) | 27.0% (75.2%) |
| HERWIG | 46.7% | 40.8% (87.4%) | 37.8% (92.7%) | 28.6% (75.7%) |
| PYTHIA | 46.6% | 37.9% (81.3%) | 32.2% (85.0%) | 24.4% (75.8%) |

**Table 5**. Comparison of the predicted selection efficiency after successive application of cuts, as obtained by fixed order calculations and event generators. Between parentheses we give the efficiency due to a single cut, after all previous cuts have been applied. The event generator predictions correspond to the parton level only, i.e., no hadronization and underlying event effects are included. The first column lists the lepton selection ("trigger") efficiencies, the second (third) columns give the results when also the jet-veto (isolation) cuts are applied in sequence and the last column lists the results after applying all remaining cuts.

Depending on the scale choice the difference ranges between 12 and 21%.

For a better understanding of the results of table 4, we now analyze the efficiency of individual cuts, applied in turn. The results are given in table 5, where the efficiencies due to a specific cut only (after all previous cuts have been applied) are presented between parentheses. We observe the following:

- When only the cuts for lepton selection are applied ("Trigger"), we generally find very good agreement of all calculations for the corresponding efficiency. In detail, MC@NLO and NNLO yield almost identical efficiencies, while HERWIG and PYTHIA give a slightly higher efficiency.

| $\sigma_{\rm acc}/\sigma_{\rm incl}$ | Trigger | + Jet-Veto | + Isolation | All Cuts |
|---|---|---|---|---|
| MC@NLO (Parton) | 44.4% | 38.1% | 35.3% | 26.5% |
| MC@NLO (Hadron) | 44.6% | 39.6% | 37.4% | 28.3% |
| MC@NLO (Had + UE) | 44.6% | 39.4% | 36.5% | 27.6% |
| PYTHIA (Parton) | 46.6% | 37.9% | 32.2% | 24.4% |
| PYTHIA (Had + UE) | 44.5% | 37.2% | 31.3% | 23.8% |

**Table 6**. Selection efficiency obtained with MC@NLO ($\mu = m_H/2$) and PYTHIA after successive application of cuts. The first row gives the results for the purely partonic MC@NLO simulation, in the second it is complemented by the cluster hadronization model as implemented in HERWIG, and in the third an underlying event model (JIMMY) is added to the simulation. For PYTHIA the inbuilt hadronization and underlying event models are applied simultaneously.

- The veto on two or more central jets is a rather critical cut for the achievable accuracy of the efficiency estimation. This "preselection" cut has been used in the recent Tevatron studies. The efficiency of the jet-veto alone, after trigger cuts, varies significantly at NNLO by about 5%. As discussed in section 5, this is due to the larger scale variation of the inclusive NNLO cross-section, while at the same time the accepted cross-section after the jet-veto application is more stable. For $\mu = m_{\rm H}/2$, where the fixed order expansion demonstrates a faster convergence, we find that the jet-veto efficiency at NNLO is in very good agreement with MC@NLO and HERWIG. PYTHIA, which is the main tool used in the Tevatron analysis, predicts an efficiency which is smaller by 6% for $\mu = m_{\rm H}/2$.

- PYTHIA also predicts a smaller efficiency by about 8% for the isolation cut. HERWIG, MC@NLO and the NNLO calculation are consistent, taking into account scale variations.

- The efficiency of the remaining cuts is very similar in all computations. After preselection, PYTHIA, rescaled with an inclusive NNLO $K$-factor, predicts between 12 and 21% less signal events than the NNLO computation.

The sensitivity of event generator predictions to cuts that restrict hadronic activity requires careful investigation. In particular, it is important to study the effect of hadronization and the underlying event on the efficiency. We have performed such an analysis in the case of MC@NLO, where hadronization effects are modeled by HERWIG and the underlying event is simulated by interfacing to the JIMMY package [66], and also for PYTHIA, where the hadronization and underlying event modelling is inbuilt. The results are given in table 6. We find only minor differences at the 1% level, which leads us to the conclusion that the differences observed with PYTHIA are rather related to its matrix element and parton shower implementation.
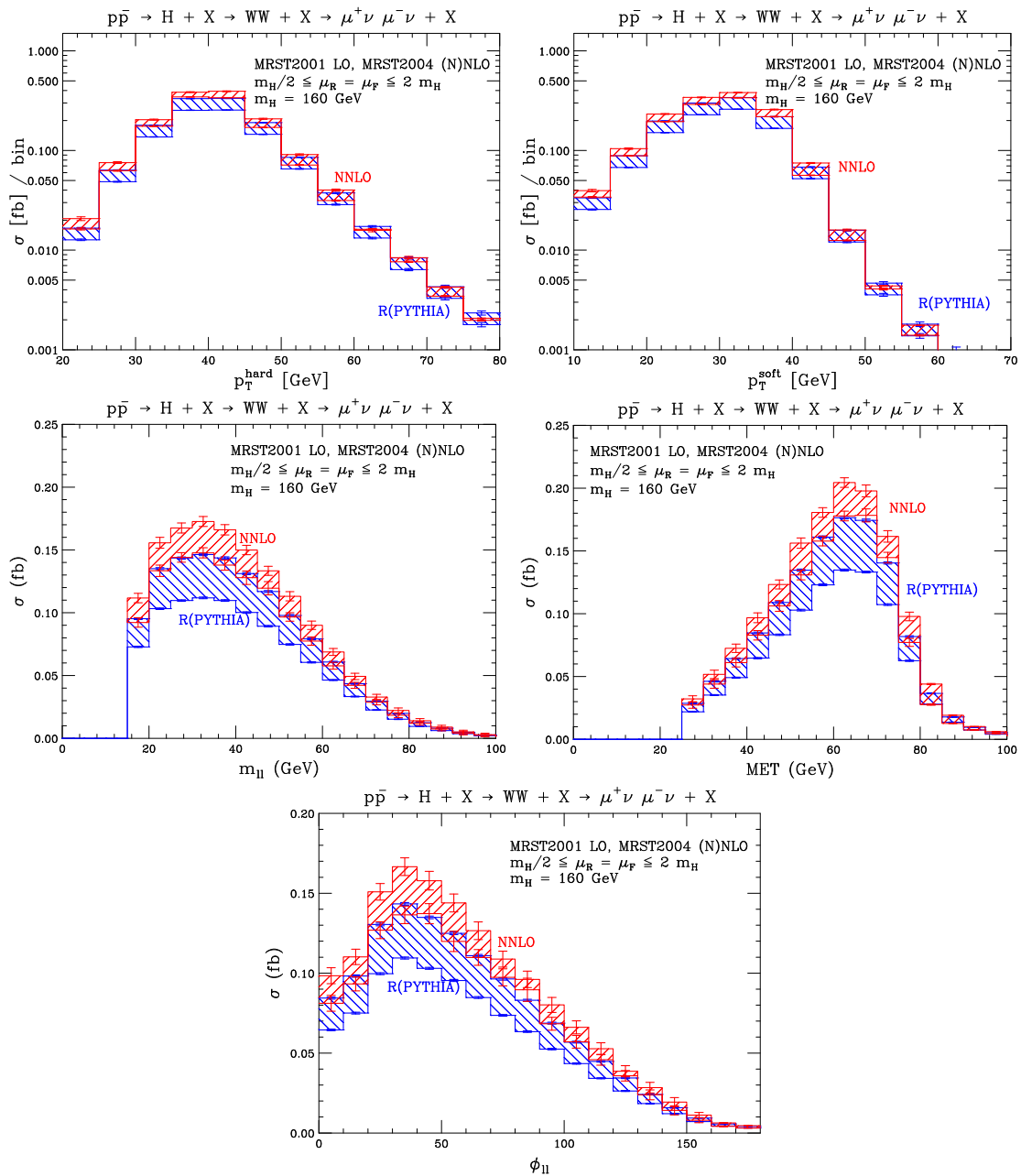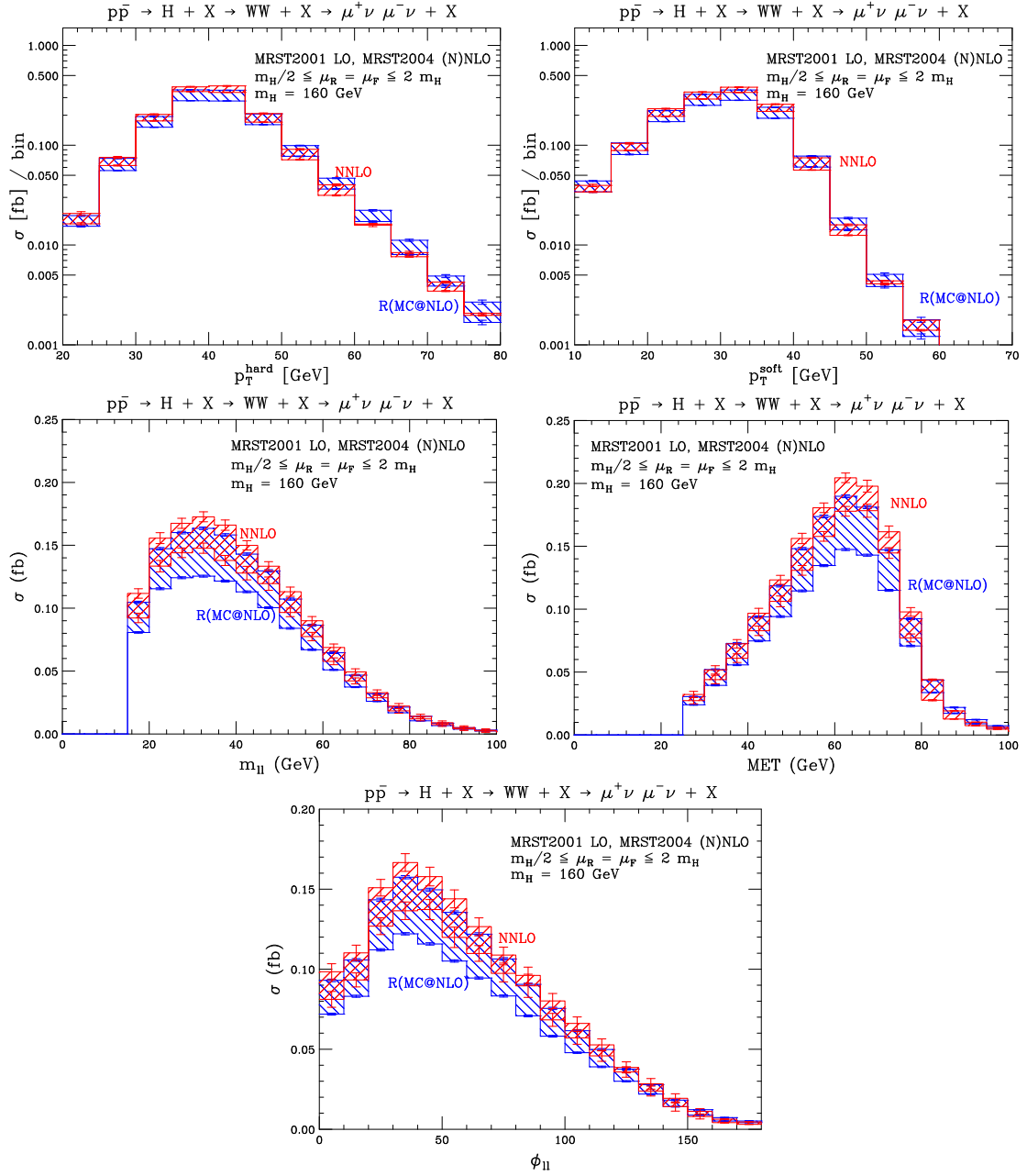
**Figure 4**. Kinematic distributions obtained at NNLO in perturbative QCD and with PYTHIA. The PYTHIA results are rescaled by an inclusive $K$-factor in order to reproduce the inclusive cross section at NNLO. Shown are the transverse momentum of the leading ($p_T^{\text{hard}}$) and trailing lepton ($p_T^{\text{soft}}$), the invariant mass of the two leptons ($m_{ll}$), the transverse missing energy (MET) and the azimuthal separation of the two charged leptons in the transverse plane ($\phi_{\ell\ell}$).

**Figure 5**. Kinematic distributions obtained at NNLO in perturbative QCD and with MC@NLO. The MC@NLO results are rescaled by an inclusive $K$-factor in order to reproduce the inclusive cross section at NNLO. Shown are the transverse momentum of the leading ($p_T^{\text{hard}}$) and trailing lepton ($p_T^{\text{soft}}$), the invariant mass of the two leptons ($m_{ll}$), the transverse missing energy (MET) and the azimuthal separation of the two charged leptons in the transverse plane ($\phi_{\ell\ell}$).
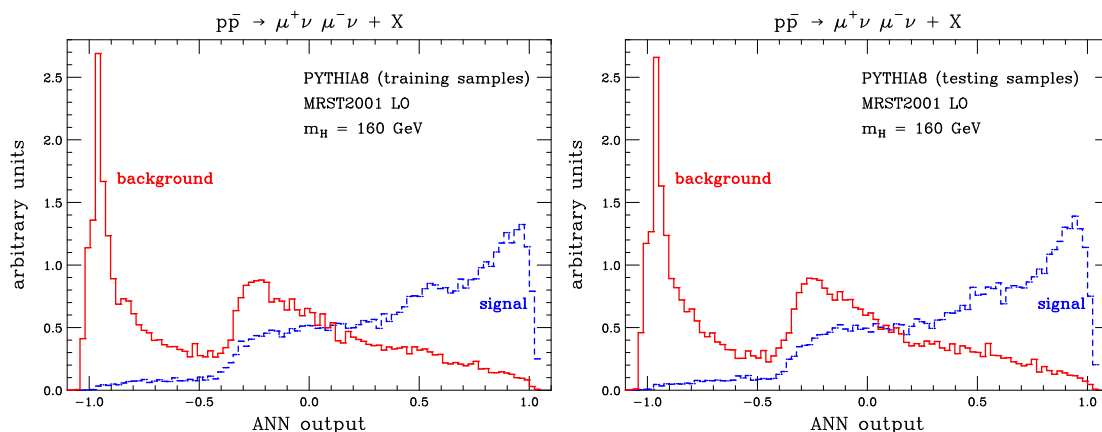
**Figure 6**. Distribution of the ANN output variable coming from the ANN construction procedure. On the left, the distribution for the training sample, on the right for the testing sample.

## 8 Artificial Neural Network

The current experimental analysis at the Tevatron attempts to distinguish a very small number of events from a considerably larger background. For such a task, the use of advanced statistical methods is necessary. An integral part of the experimental studies are distributions of discrimination variables, defined via artificial neural networks (ANN). It is clear that such techniques will become an indispensable tool in many future studies at the Tevatron and at the LHC, optimizing the sensitivity of the experiments.

To the best of our knowledge, so far there has been no study of how the distributions of ANN outputs are modified at higher orders in perturbation theory. Here we present for the first time an ANN output distribution, computed at fixed order in perturbation theory, beyond the leading order.

In order to study these higher-order effects on the outcome variable, we have built an ANN with the tool TMVA v. 3.9.2. [67] based on the Data Analysis Framework ROOT v. 5.21.02 [68]. In the construction (the so-called training) of the ANN the user has to provide a set of signal and background events, as well as a list of input variables. In our study we use the variables defined in section 6 as input variables. Based on the techniques of Multilayer Perceptrons, the ANN then builds an output variable, which is basically a non-linear function of the input variables. Since our study is based on Monte Carlo truth information, we restrict the set of background to processes that have the same final state signature as the signal, i.e. to continuum WW background and top-pair production. For both of these processes, as well as for the signal process, we generate a large enough event sample ($\sim$ 50000 events after pre-selection) with the LO parton-shower Monte Carlo PYTHIA8 [56], and use half of the samples to train the ANN. The other half is used in the so-called testing step.

Figure 6 shows the ANN output for the signal and background samples, for the training (left) and the testing (right) samples. The comparison of the training and testing
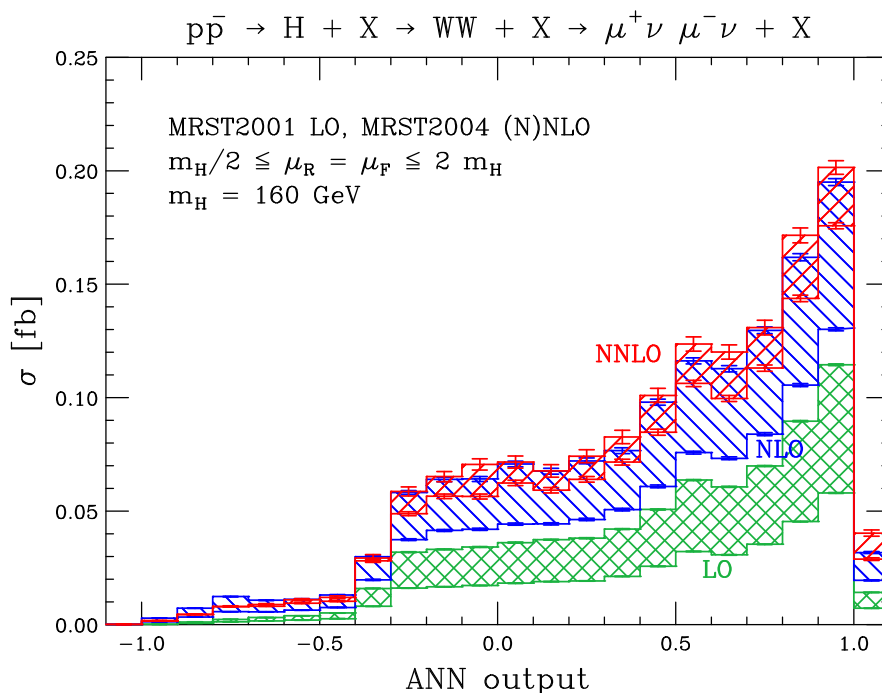
**Figure 7**. Distribution of the ANN output variable, computed at LO, NLO and NNLO in perturbation theory. The bands indicate the scale uncertainties.

distributions serves as a verification that the ANN has not been over-trained, i.e. tuned to statistical effects in the training sample. The discrimination power of the ANN variable can be seen clearly. While the background distribution peaks at low values,[2] the signal events populate the high value range. Distributions like this can serve to distinguish background from possible signal events, either by cutting on the ANN output, or by using the shape of the distribution to decide whether the observed event set consists of background only or background and signal events.

In figure 7 we present the distribution of the ANN output for the signal in fixed-order perturbation theory, computed at LO, NLO and NNLO. We find significant radiative corrections, which however are consistent in magnitude with those for the accepted cross section after preselection cuts.

In figure 8 we compare the ANN distribution obtained at NNLO and with MC@NLO. Again we find a very good agreement between the fixed order calculation and the MC@NLO prediction, when the latter is rescaled with a $K$-factor in order to reproduce the total inclusive cross-section.

Finally, in figure 9 we compare the ANN distribution obtained at NNLO QCD and with PYTHIA. We see that PYTHIA, even after rescaling with an inclusive $K$-factor, yields predictions which are smaller by 12-20%, depending on the chosen bin. This difference can be traced back to the difference in efficiency already observed at the level of the selection cuts placed on the kinematic input distributions.

---

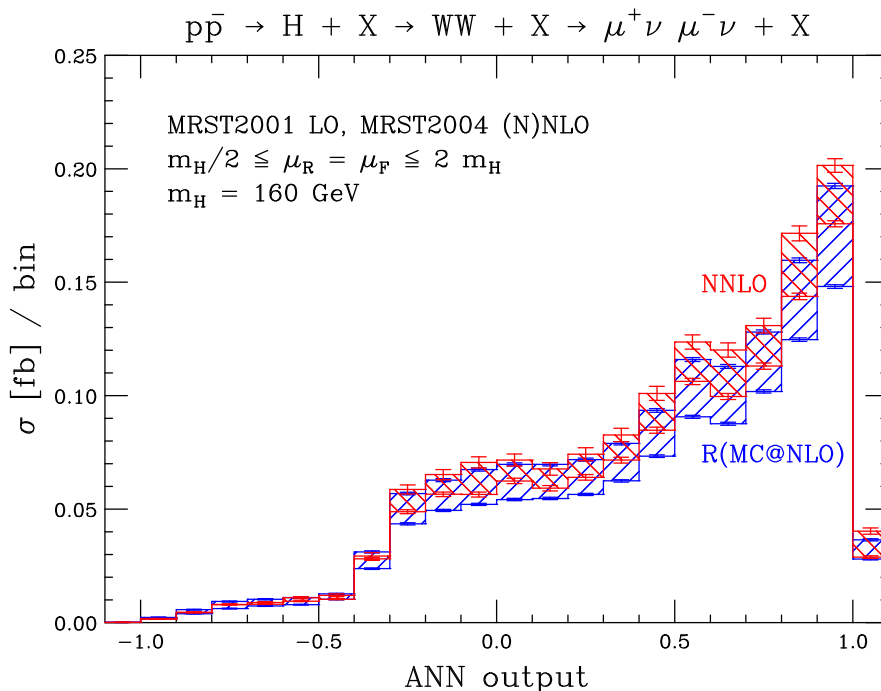[2]The background peaks around $-1.0$ and $-0.3$ arise mainly from $t\bar{t}$ and $WW$ respectively.

**Figure 8**. Distribution of the ANN output variable, computed at NNLO in perturbation theory and with MC@NLO. The MC@NLO result is rescaled by an inclusive $K$-factor in order to reproduce the inclusive cross section at NNLO. The bands indicate the scale uncertainties.

Note that we have not included any hadronic variable as an input to the ANN. It is clear that stable perturbative patterns are obtained as long as we apply cuts on "leptonic" variables only. However, adding a hadronic variable to the list of ANN inputs could produce results that are very sensitive to the details of the modeling of the hadronic activity in the event generators used for the training of the network.

## 9  Conclusions

In this paper we have studied higher-order QCD effects in the search for a Higgs boson of mass $m_H = 160\,\text{GeV}$ at the Tevatron. We have considered a definite set of preselection cuts that we believe capture the essential features of the CDF and DØ analyses. We have studied the impact of higher order corrections on a set of kinematical distributions of the final state leptons. We have then compared these distributions, computed up to NNLO in QCD perturbation theory, to those obtained with the PYTHIA, HERWIG and MC@NLO event generators. The comparison of distributions does not show significant differences, and this is confirmed by a more sophisticated analysis we have performed based on the training of our own ANN.

For the ANN analysis we used only leptonic input variables, in order to reduce sensitivity to the modelling of hadronic activity and to allow perturbative evaluation of the output
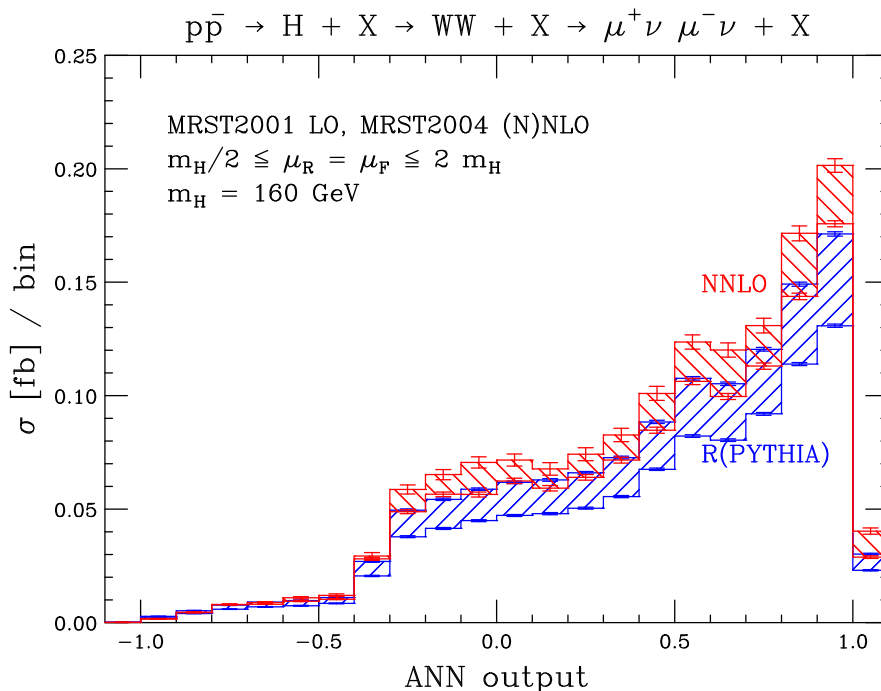
**Figure 9**. Distribution of the ANN output variable, computed at NNLO in perturbation theory and with PYTHIA. The PYTHIA result is rescaled by an inclusive $K$-factor in order to reproduce the inclusive cross section at NNLO. The bands indicate the scale uncertainties.

distribution. These features are also necessary for the reliable estimation of theoretical uncertainties in experimental ANN analyses.

We have also compared the efficiency of the experimental cuts obtained in NNLO QCD to those obtained with PYTHIA, HERWIG and MC@NLO. The efficiencies obtained with HERWIG and MC@NLO are consistent with that obtained at NNLO. The MC@NLO acceptance is slightly smaller than the NNLO acceptance, by $4-14\%$, while the acceptance of HERWIG differs from the NNLO prediction by $-3\%$ to $+8\%$. In contrast, we find that the acceptance computed with PYTHIA is between $12\%$ and $21\%$ smaller than the NNLO acceptance, depending on the choice of the factorization and renormalization scale. This result is not significantly altered by hadronization and underlying event and appears instead to be related to the matrix element and parton shower implementation in PYTHIA itself. Since the Tevatron analyses are based on PYTHIA, we believe that this effect could be important and requires a more detailed investigation within the framework of the full experimental analysis.

Relevant to the experimental analysis, we have remarked that the combination in quadrature of the theoretical errors due to the parton distributions and scale variations in refs. [2, 3] implies that the theoretical uncertainty on the total cross section used there is likely to be underestimated. We also pointed out that a reweighting of parton shower Monte-Carlos to match the fixed-order Higgs $p_T$ distribution is not appropriate for events with a low Higgs $p_T$ value. Finally, we have demonstrated that a reliable estimation of the

theoretical uncertainty for Higgs signal cross-sections with defined jet multiplicities requires dedicated fixed order computations for each multiplicity. The theoretical uncertainty in each jet-bin is different from the theoretical uncertainty of the total cross-section.

## Acknowledgments

## References

[1] CDF collaboration, T. Aaltonen et al., *Search for a Higgs Boson Decaying to Two W Bosons at CDF*, *Phys. Rev. Lett.* **102** (2009) 021802 [arXiv:0809.3930] [SPIRES].

[2] CDF collaboration, *Search for H → WW production at CDF using 3.0 fb⁻¹ of data*, CDF conference note 9500 (2009).

[3] D0 collaboration, *Search for Higgs boson production in dilepton plus missing transverse energy final states with 3.0–4.2 fb⁻¹ of p$\bar{p}$ collisions at $\sqrt{s}$ = 1.96 TeV*, D0 conference note 5871 (2009).

[4] TEVATRON NEW PHENOMENA HIGGS WORKING GROUP, CDF AND D0 collaboration, G. Bernardi et al., *Combined CDF and D0 Upper Limits on Standard Model Higgs Boson Production at High Mass* $(155 - 200 - GeV/c^{2)}$ *with 3 fb⁻¹ of data*, arXiv:0808.0534 [SPIRES].

[5] TEVATRON NEW PHENOMENA HIGGS WORKING GROUP, CDF AND D0 collaboration, *Combined CDF and DZero Upper Limits on Standard Model Higgs-Boson Production with up to 4.2 fb-1 of Data*, arXiv:0903.4001 [SPIRES].

[6] S. Dawson, *Radiative corrections to Higgs boson production*, *Nucl. Phys.* **B 359** (1991) 283 [SPIRES].

[7] A. Djouadi, M. Spira and P.M. Zerwas, *Production of Higgs bosons in proton colliders: QCD corrections*, *Phys. Lett.* **B 264** (1991) 440 [SPIRES].

[8] M. Spira, A. Djouadi, D. Graudenz and P.M. Zerwas, *Higgs boson production at the LHC*, *Nucl. Phys.* **B 453** (1995) 17 [hep-ph/9504378] [SPIRES].

[9] R.V. Harlander and W.B. Kilgore, *Next-to-next-to-leading order Higgs production at hadron colliders*, *Phys. Rev. Lett.* **88** (2002) 201801 [hep-ph/0201206] [SPIRES].

[10] C. Anastasiou and K. Melnikov, *Higgs boson production at hadron colliders in NNLO QCD*, *Nucl. Phys.* **B 646** (2002) 220 [hep-ph/0207004] [SPIRES].

[11] V. Ravindran, J. Smith and W.L. van Neerven, *NNLO corrections to the total cross section for Higgs boson production in hadron hadron collisions*, *Nucl. Phys.* **B 665** (2003) 325 [hep-ph/0302135] [SPIRES].

[12] S. Catani, D. de Florian, M. Grazzini and P. Nason, *Soft-gluon resummation for Higgs boson production at hadron colliders*, *JHEP* **07** (2003) 028 [hep-ph/0306211] [SPIRES].

[13] S. Moch and A. Vogt, *Higher-order soft corrections to lepton pair and Higgs boson production*, *Phys. Lett.* **B 631** (2005) 48 [hep-ph/0508265] [SPIRES].

[14] E. Laenen and L. Magnea, *Threshold resummation for electroweak annihilation from DIS data*, *Phys. Lett.* **B 632** (2006) 270 [hep-ph/0508284] [SPIRES].

[15] A. Idilbi, X.-d. Ji, J.-P. Ma and F. Yuan, *Threshold resummation for Higgs production in effective field theory*, *Phys. Rev.* **D 73** (2006) 077501 [`hep-ph/0509294`] [SPIRES].

[16] V. Ravindran, *On Sudakov and soft resummations in QCD*, *Nucl. Phys.* **B 746** (2006) 58 [`hep-ph/0512249`] [SPIRES].

[17] V. Ravindran, *Higher-order threshold effects to inclusive processes in QCD*, *Nucl. Phys.* **B 752** (2006) 173 [`hep-ph/0603041`] [SPIRES].

[18] V. Ravindran, J. Smith and W.L. van Neerven, *QCD threshold corrections to di-lepton and Higgs rapidity distributions beyond $N^2$ LO*, *Nucl. Phys.* **B 767** (2007) 100 [`hep-ph/0608308`] [SPIRES].

[19] V. Ahrens, T. Becher, M. Neubert and L.L. Yang, *Renormalization-Group Improved Prediction for Higgs Production at Hadron Colliders*, *Eur. Phys. J.* **C 62** (2009) 333 [`arXiv:0809.4283`] [SPIRES].

[20] G. Degrassi and F. Maltoni, *Two-loop electroweak corrections to Higgs production at hadron colliders*, *Phys. Lett.* **B 600** (2004) 255 [`hep-ph/0407249`] [SPIRES].

[21] U. Aglietti, R. Bonciani, G. Degrassi and A. Vicini, *Two-loop light fermion contribution to Higgs production and decays*, *Phys. Lett.* **B 595** (2004) 432 [`hep-ph/0404071`] [SPIRES].

[22] U. Aglietti, R. Bonciani, G. Degrassi and A. Vicini, *Two-loop electroweak corrections to Higgs production in proton proton collisions*, `hep-ph/0610033` [SPIRES].

[23] S. Actis, G. Passarino, C. Sturm and S. Uccirati, *NLO Electroweak Corrections to Higgs Boson Production at Hadron Colliders*, *Phys. Lett.* **B 670** (2008) 12 [`arXiv:0809.1301`] [SPIRES].

[24] S. Actis, G. Passarino, C. Sturm and S. Uccirati, *NNLO Computational Techniques: the Cases $H \to \gamma\gamma$ and $H \to gg$*, *Nucl. Phys.* **B 811** (2009) 182 [`arXiv:0809.3667`] [SPIRES].

[25] C. Anastasiou, R. Boughezal and F. Petriello, *Mixed QCD-electroweak corrections to Higgs boson production in gluon fusion*, *JHEP* **04** (2009) 003 [`arXiv:0811.3458`] [SPIRES].

[26] D. de Florian and M. Grazzini, *Higgs production through gluon fusion: updated cross sections at the Tevatron and the LHC*, *Phys. Lett.* **B 674** (2009) 291 [`arXiv:0901.2427`] [SPIRES].

[27] A. Bredenstein, A. Denner, S. Dittmaier and M.M. Weber, *Precise predictions for the Higgs-boson decay $H \to W W/Z Z \to 4$ leptons*, *Phys. Rev.* **D 74** (2006) 013004 [`hep-ph/0604011`] [SPIRES].

[28] A. Djouadi, J. Kalinowski and M. Spira, *HDECAY: A program for Higgs boson decays in the standard model and its supersymmetric extension*, *Comput. Phys. Commun.* **108** (1998) 56 [`hep-ph/9704448`] [SPIRES].

[29] M. Dittmar and H.K. Dreiner, *How to find a Higgs boson with a mass between 155 GeV–180 GeV at the LHC*, *Phys. Rev.* **D 55** (1997) 167 [`hep-ph/9608317`] [SPIRES].

[30] C. Anastasiou, L.J. Dixon, K. Melnikov and F. Petriello, *Dilepton rapidity distribution in the Drell-Yan process at NNLO in QCD*, *Phys. Rev. Lett.* **91** (2003) 182002 [`hep-ph/0306192`] [SPIRES].

[31] C. Anastasiou, L.J. Dixon, K. Melnikov and F. Petriello, *High precision QCD at hadron colliders: Electroweak gauge boson rapidity distributions at NNLO*, *Phys. Rev.* **D 69** (2004) 094008 [`hep-ph/0312266`] [SPIRES].

[32] C. Anastasiou, K. Melnikov and F. Petriello, *Real radiation at NNLO: $e^+e^- \to 2$jets through $O(\alpha_s^2)$*, *Phys. Rev. Lett.* **93** (2004) 032002 [`hep-ph/0402280`] [SPIRES].

[33] C. Anastasiou, K. Melnikov and F. Petriello, *Higgs boson production at hadron colliders: differential cross sections through next-to-next-to-leading order*, *Phys. Rev. Lett.* **93** (2004) 262002 [hep-ph/0409088] [SPIRES].

[34] S. Weinzierl, *The forward-backward asymmetry at NNLO revisited*, *Phys. Lett.* **B 644** (2007) 331 [hep-ph/0609021] [SPIRES].

[35] A. Gehrmann-De Ridder, T. Gehrmann, E.W.N. Glover and G. Heinrich, *NNLO moments of event shapes in $e^+e^-$ annihilation*, *JHEP* **05** (2009) 106 [arXiv:0903.4658] [SPIRES].

[36] A. Gehrmann-De Ridder, T. Gehrmann, E.W.N. Glover and G. Heinrich, *Jet rates in electron-positron annihilation at $O(\alpha_s^3)$ in QCD*, *Phys. Rev. Lett.* **100** (2008) 172001 [arXiv:0802.0813] [SPIRES].

[37] G. Dissertori et al., *First determination of the strong coupling constant using NNLO predictions for hadronic event shapes in $e^+e^-$ annihilations*, *JHEP* **02** (2008) 040 [arXiv:0712.0327] [SPIRES].

[38] A. Gehrmann-De Ridder, T. Gehrmann, E.W.N. Glover and G. Heinrich, *NNLO corrections to event shapes in $e^+e^-$ annihilation*, *JHEP* **12** (2007) 094 [arXiv:0711.4711] [SPIRES].

[39] A. Gehrmann-De Ridder, T. Gehrmann, E.W.N. Glover and G. Heinrich, *Second-order QCD corrections to the thrust distribution*, *Phys. Rev. Lett.* **99** (2007) 132002 [arXiv:0707.1285] [SPIRES].

[40] S. Weinzierl, *The infrared structure of $e^+e^- \to 3$ jets at NNLO reloaded*, *JHEP* **07** (2009) 009 [arXiv:0904.1145] [SPIRES].

[41] S. Weinzierl, *Event shapes and jet rates in electron-positron annihilation at NNLO*, *JHEP* **06** (2009) 041 [arXiv:0904.1077] [SPIRES].

[42] S. Weinzierl, *NNLO corrections to 3-jet observables in electron-positron annihilation*, *Phys. Rev. Lett.* **101** (2008) 162001 [arXiv:0807.3241] [SPIRES].

[43] C. Anastasiou, K. Melnikov and F. Petriello, *Fully differential Higgs boson production and the di- photon signal through next-to-next-to-leading order*, *Nucl. Phys.* **B 724** (2005) 197 [hep-ph/0501130] [SPIRES];
http://www.phys.hawaii.edu/~kirill/FEHiP.htm.

[44] S. Catani and M. Grazzini, *An NNLO subtraction formalism in hadron collisions and its application to Higgs boson production at the LHC*, *Phys. Rev. Lett.* **98** (2007) 222002 [hep-ph/0703012] [SPIRES].

[45] C. Anastasiou, G. Dissertori and F. Stockli, *NNLO QCD predictions for the $H \to WW \to \ell\nu\ell\nu$ signal at the LHC*, *JHEP* **09** (2007) 018 [arXiv:0707.2373] [SPIRES].

[46] M. Grazzini, *NNLO predictions for the Higgs boson signal in the $H \to WW \to l\nu l\nu$ and $H \to ZZ \to 4l$ decay channels*, *JHEP* **02** (2008) 043 [arXiv:0801.3232] [SPIRES].

[47] K. Melnikov and F. Petriello, *Electroweak gauge boson production at hadron colliders through $O(\alpha_s^2)$*, *Phys. Rev.* **D 74** (2006) 114017 [hep-ph/0609070] [SPIRES].

[48] K. Melnikov and F. Petriello, *The W boson production cross section at the LHC through $O(\alpha_s^2)$*, *Phys. Rev. Lett.* **96** (2006) 231803 [hep-ph/0603182] [SPIRES].

[49] S. Catani, L. Cieri, G. Ferrera, D. de Florian and M. Grazzini, *Vector boson production at hadron colliders: a fully exclusive QCD calculation at NNLO*, arXiv:0903.2120 [SPIRES].

[50] C. Anastasiou, K. Melnikov and F. Petriello, *A new method for real radiation at NNLO*, *Phys. Rev.* **D 69** (2004) 076010 [hep-ph/0311311] [SPIRES].

[51] C. Anastasiou, G. Dissertori, F. Stockli and B.R. Webber, *QCD radiation effects on the H → WW → ℓnuℓnu signal at the LHC*, *JHEP* **03** (2008) 017 [arXiv:0801.2682] [SPIRES].

[52] G. Bozzi, S. Catani, D. de Florian and M. Grazzini, *Transverse-momentum resummation and the spectrum of the Higgs boson at the LHC*, *Nucl. Phys.* **B 737** (2006) 73 [hep-ph/0508068] [SPIRES].

[53] S. Frixione and B.R. Webber, *Matching NLO QCD computations and parton shower simulations*, *JHEP* **06** (2002) 029 [hep-ph/0204244] [SPIRES]; *The MC@NLO 3.4 Event Generator*, arXiv:0812.0770 [SPIRES].

[54] G. Corcella et al., *HERWIG 6.5: an event generator for Hadron Emission Reactions With Interfering Gluons (including supersymmetric processes)*, *JHEP* **01** (2001) 010 [hep-ph/0011363] [SPIRES];
*HERWIG 6.5 release note*, hep-ph/0210213 [SPIRES].

[55] T. Sjöstrand, S. Mrenna and P. Skands, *A Brief Introduction to PYTHIA 8.1*, *Comput. Phys. Commun.* **178** (2008) 852 [arXiv:0710.3820] [SPIRES].

[56] T. Sjöstrand, S. Mrenna and P. Skands, *PYTHIA 6.4 Physics and Manual*, *JHEP* **05** (2006) 026 [hep-ph/0603175] [SPIRES].

[57] G. Davatz, G. Dissertori, M. Dittmar, M. Grazzini and F. Pauss, *Effective K-factors for g g → H → W W → ℓνℓν at the LHC*, *JHEP* **05** (2004) 009 [hep-ph/0402218] [SPIRES].

[58] G. Davatz et al., *Combining Monte Carlo generators with next-to-next-to-leading order calculations: Event reweighting for Higgs boson production at the LHC*, *JHEP* **07** (2006) 037 [hep-ph/0604077] [SPIRES].

[59] T. Gleisberg et al., *SHERPA 1.alpha, a proof-of-concept version*, *JHEP* **02** (2004) 056 [hep-ph/0311263] [SPIRES].

[60] A.D. Martin, W.J. Stirling, R.S. Thorne and G. Watt, *Parton distributions for the LHC*, arXiv:0901.0002 [SPIRES].

[61] C. Anastasiou, S. Beerli, S. Bucherer, A. Daleo and Z. Kunszt, *Two-loop amplitudes and master integrals for the production of a Higgs boson via a massive quark and a scalar-quark loop*, *JHEP* **01** (2007) 082 [hep-ph/0611236] [SPIRES].

[62] C. Balázs, M. Grazzini, J. Huston, A. Kulesza and I. Puljak, *A comparison of predictions for SM Higgs boson production at the LHC*, hep-ph/0403052 [SPIRES].

[63] S. Catani, Y.L. Dokshitzer, M.H. Seymour and B.R. Webber, *Longitudinally invariant $K_t$ clustering algorithms for hadron hadron collisions*, *Nucl. Phys.* **B 406** (1993) 187 [SPIRES].

[64] S.D. Ellis and D.E. Soper, *Successive combination jet algorithm for hadron collisions*, *Phys. Rev.* **D 48** (1993) 3160 [hep-ph/9305266] [SPIRES].

[65] J.M. Campbell, R.K. Ellis and G. Zanderighi, *Next-to-leading order Higgs + 2 jet production via gluon fusion*, *JHEP* **10** (2006) 028 [hep-ph/0608194] [SPIRES].

[66] J.M. Butterworth, J.R. Forshaw and M.H. Seymour, *Multiparton interactions in photoproduction at HERA*, *Z. Phys.* **C 72** (1996) 637 [hep-ph/9601371] [SPIRES].

[67] *TMVA: Toolkit for Multivariate Data Analysis with ROOT*, http://tmva.sourceforge.net/.

[68] *ROOT, A Data Analysis Framework*, http://root.cern.ch.